Springtime Export of Arctic Sea Ice Influences Phytoplankton Production in the Greenland Sea

N. Mayot, P. A. Matrai, A. Arjona, S. Bélanger, C. Marchese, T. Jaegler, M. Ardyna, M. Steele

JGR Oceans

RESEARCH ARTICLE
10.1029/2019JC015799

Key Points:
- A positive relationship exists between exported Arctic sea ice and the sea ice distribution in the Greenland Sea
- High (low) springtime export of Arctic sea ice may increase (reduce) the stratification of the Greenland Basin
- A strong (weak) salinity stratification of the Greenland Basin induces an early (late) phytoplankton spring bloom and primary production

Supporting Information:
- Supporting Information S1

Correspondence to:
N. Mayot and P. Matrai,
n.mayot@uea.ac.uk;
pmatrai@bigelow.org

Citation:
Mayot, N., Matrai, P. A., Arjona, A., Bélanger, S., Marchese, C., Jaegler, T., et al. (2020). Springtime export of Arctic sea ice influences phytoplankton production in the Greenland Sea. *Journal of Geophysical Research: Oceans*, *125*, e2019JC015799. https://doi.org/10.1029/2019JC015799

Received 25 OCT 2019
Accepted 27 FEB 2020
Accepted article online 3 MAR 2020

Springtime Export of Arctic Sea Ice Influences Phytoplankton Production in the Greenland Sea

N. Mayot[1], P. A. Matrai[1], A. Arjona[1,2], S. Bélanger[3,4], C. Marchese[3,4], T. Jaegler[4], M. Ardyna[5,6], and M. Steele[7]

[1]Bigelow Laboratory for Ocean Sciences, East Boothbay, ME, USA, [2]Harvard University, Cambridge, MA, USA, [3]Département de Biologie, Chimie et Géographie, groupe BORÉAS et Québec-Océan, Université du Québec à Rimouski, Rimouski, Québec, Canada, [4]ARCTUS inc., Rimouski, Québec, Canada, [5]Department of Earth System Science, Stanford University, Stanford, CA, USA, [6]Laboratoire d'Océanographie de Villefranche (LOV), Sorbonne Université and CNRS, Villefranche-sur-mer, France, [7]Applied Physics Laboratory, University of Washington, Seattle, WA, USA

Abstract Climate model projections suggest a substantial decrease of sea ice export into the outflow areas of the Arctic Ocean over the 21st century. Fram Strait, located in the Greenland Sea sector, is the principal gateway for ice export from the Arctic Ocean. The consequences of lower sea ice flux through Fram Strait on ocean dynamics and primary production in the Greenland Sea remain unknown. By using the most recent 16 years (2003–2018) of satellite imagery available and hydrographic in situ observations, the role of exported Arctic sea ice on water column stratification and phytoplankton production in the Greenland Sea is evaluated. Years with high Arctic sea ice flux through Fram Strait resulted in high sea ice concentration in the Greenland Sea, stronger water column stratification, and an earlier spring phytoplankton bloom associated with high primary production levels. Similarly, years with low Fram Strait ice flux were associated with a weak water column stratification and a delayed phytoplankton spring bloom. This work emphasizes that sea ice and phytoplankton production in subarctic "outflow seas" can be strongly influenced by changes occurring in the Arctic Ocean.

Plain Language Summary As the Arctic atmosphere and ocean warm, Arctic sea ice continues to decline. The Greenland Sea (to the east of Greenland) is heavily influenced by sea ice leaving the Arctic Ocean. In this study, we address the impacts of sea ice exiting the Arctic on the development of free-floating microscopic algae in the Greenland Sea. For this, we analyzed 16 years of data from satellite images and autonomous ocean robots. Our results reveal that changes in the quantity of sea ice leaving the Arctic Ocean in spring modify the environment and development of microscopic algae. These algae are important because they capture carbon dioxide and support ocean life; this paper can help to predict how they will respond to the ongoing environmental changes occurring in the Arctic.

1. Introduction

Arctic marine ecosystems are particularly sensitive to climate change, facing a faster warming than some other oceanic environments (Meredith et al., 2019; Osborne et al., 2018; Serreze & Barry, 2014). Furthermore, since the 2000s, the rapid decline in sea ice and increase in liquid freshwater storage also modify the Arctic freshwater reservoirs (see reviews from Carmack et al., 2016; Haine et al., 2015 and references therein). The projected climate changes for the Arctic in the 21st century will amplify the ongoing warming and freshening of the Arctic Ocean and the shrinking and thinning of the Arctic sea ice during all seasons (Haine et al., 2015). The growing concern about the observed and predicted modifications of the Arctic Ocean has been extended to the outflow areas of the Arctic Ocean, due, in particular, to the potential reduction in sea ice export and increase in liquid freshwater export through Fram and Davis Straits (e.g., Vavrus et al., 2012).

These changes in the Arctic Ocean and Arctic outflows have several physical and biogeochemical consequences (e.g., Carmack et al., 2016) that could, for example, reduce the deep convection in the Nordic Seas and slow down the Atlantic Meridional Overturning Circulation during the 21st century (Arzel et al., 2008; Brakstad et al., 2018; Jahn & Holland, 2013). Regarding phytoplankton, the long-term decline

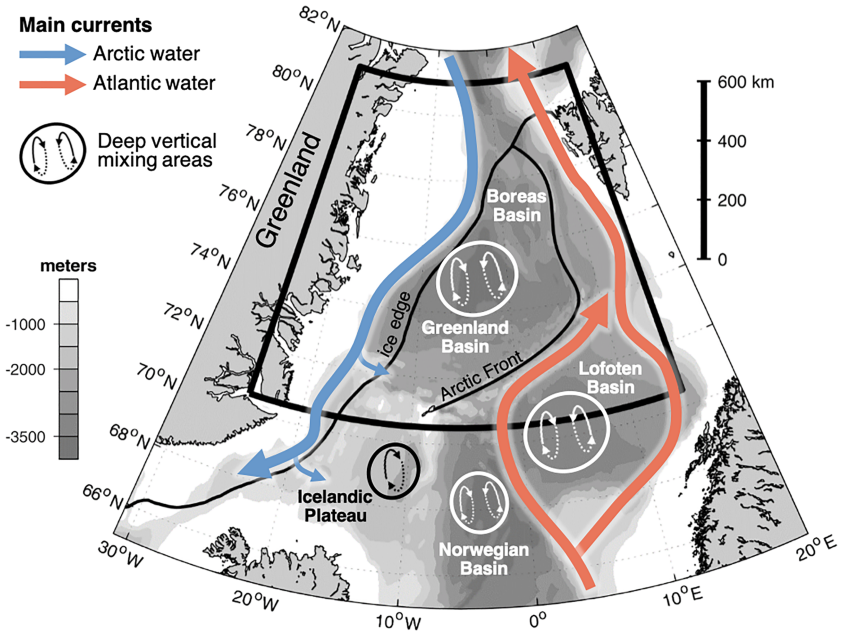

Figure 1. Nordic Seas bathymetry, with locations of the main currents, the Arctic front, the ice edge in April (15% of sea ice concentration), and deep vertical mixing areas. The black box represents the location of the study area.

in phytoplankton productivity in the subarctic Atlantic Ocean (above 55°N) over the past two centuries may be related to the freshening of the North Atlantic and reduction of the Atlantic Meridional Overturning Circulation (Osman et al., 2019). Indeed, there is growing evidence showing connections between phytoplankton dynamics on the west side of Greenland and in the northwest Atlantic Ocean, with the freshwater coming from the Arctic Ocean and the Greenland ice sheet (e.g., Arrigo et al., 2017; Frajka-Williams & Rhines, 2010; Greene & Pershing, 2007; Joli et al., 2018; Marchese et al., 2019). Moreover, the sensitivity of phytoplankton ecology to the ongoing decline in Arctic sea ice within the Arctic Ocean itself is well known (Carmack & Wassmann, 2006; Gradinger, 1995; Macias-Fauria & Post, 2018; Wassmann et al., 2011). For example, some suggest and predict an increase in the total annual phytoplankton production on the Arctic interior shelves (Arrigo et al., 2008; Arrigo & van Dijken, 2015; Kahru et al., 2016; Slagstad et al., 2015) and under sea ice (Horvat et al., 2017), the occurrence of northern and more productive spring blooms (Renaut et al., 2018), a change in the date of the production maximum (Kahru et al., 2011), and the appearance of fall blooms in some regions (Ardyna et al., 2014).

North of the Arctic Circle (66°N), most phytoplankton production occurs in the Greenland and Barents Seas sectors and not in the central Arctic Ocean (i.e., Eurasian and Amerasian basins) or Arctic interior shelves (Pabi et al., 2008; Slagstad et al., 2015). Moreover, the Arctic seas are highly dynamic oceanic environments with significant spatial and temporal variabilities in sea ice cover and primary production (Carmack & Wassmann, 2006; Harrison et al., 2013; Skogen et al., 2007). Observational analyses are required to evaluate key physical-biological coupling processes associated with dynamic Arctic seas environments, in order to better quantify potential climate-related changes of the pan-Arctic Ocean biology and biogeochemistry in the next decades and centuries.

The Greenland Sea sector of the pan-Arctic Ocean has very high total annual phytoplankton production, due to its large permanently open water areas (Ardyna et al., 2013; Bélanger et al., 2013; Pabi et al., 2008; Sakshaug, 2004). This Arctic sector, associated with Fram Strait, is also the most exposed region to the export of Arctic sea ice and water masses (e.g., Carmack & Wassmann, 2006). The Greenland Sea, located in this sector, is a spatially complex oceanic area, with wide shelves on its western side where the outflow of Arctic waters and sea ice occurs, two basins (Greenland and Boreas Basins) at its center where deep convection processes take place, and a narrow shelf along western Svalbard (Figure 1, Longhurst, 1998). The Greenland Sea is, in addition, highly temporally dynamic, with strong intraannual and interannual variabilities in sea ice extent (e.g., Comiso et al., 2001; Germe et al., 2011) and a loitering of the ice edge during the

sea ice retreat season (Steele & Ermold, 2015). In fact, it is believed that the sea ice along the Greenland coast "extends patchily and irregularly" across the East Greenland Current and into the Greenland Sea open ocean area (Johannessen et al., 1992; Longhurst, 1998). Correspondingly, salinity in the Greenland Basin also shows such high interannual variability, even higher than the seasonal variability (Latarius & Quadfasel, 2010).

In the Greenland Sea, the freshwater content of open ocean areas is dominated by the melting of sea ice exported from the Arctic basin through Fram Strait (de Steur et al., 2015). Prior studies suggest that this surface layer of meltwater in Greenland Sea open water is the result of locally melted sea ice (i.e., a loss of solid sea ice from the East Greenland Current, Dodd et al., 2009, 2012). Even if no significant long-term trends (reduction or increase since 1930s) in ice export fluxes have yet been seen in Fram Strait, it is highly probable they will occur (e.g., Haine et al., 2015; Smedsrud et al., 2017). In fact, despite the suggested recent (since 1979) increase in Arctic sea ice export through Fram Strait (Smedsrud et al., 2017), most climatic model results predict a strong reduction in export by the end of the 21st century (Haine et al., 2015; Vavrus et al., 2012). Other studies suggest a future decrease in nutrient availability for the phytoplankton production in the Greenland Sea, owing to increased thermal stratification (Slagstad et al., 2015) and enhanced nutrient consumption upstream in the Arctic (Arrigo & van Dijken, 2015; Tremblay et al., 2015). However, less is known regarding the variability in biogeochemical processes triggered by freshwater changes (oceanic and sea ice), particularly in open ocean areas of the Greenland Sea (as opposed to coastal/fjord areas). The large interannual variability of Fram Strait sea ice flux (e.g., Kwok et al., 2004; Smedsrud et al., 2017) allows an examination of the potential coupling between ice export fluxes and physical-biogeochemical processes in the Greenland Sea region.

The spring season plays a key role in the annual cycle of the phytoplankton production occurring in the pan-Artic Ocean. Indeed, the timing, duration, and magnitude of springtime phytoplankton production have significant implications for several biogeochemical cycles (e.g., carbon export and nitrogen cycling; Tremblay et al., 2015) and the energy transfer in marine food webs with, for example, direct consequences for pan-Arctic marine ecosystems (e.g., Søreide et al., 2010). Ecologically, the Greenland Sea, together with the Irminger and Labrador Seas, forms the "Atlantic Arctic Province" of Longhurst (1998). This is the site of a very productive spring phytoplankton bloom that is generally followed by population increases of large copepods.

This study is focused on the following question: Does the interannual variability of the exported Arctic sea ice flux influence both the physical environment and phytoplankton dynamics (i.e., phenology and production) during spring in the Greenland Basin? We answer this question using both satellite and in situ biophysical observations over the last 16 years (from 2003 to 2018).

2. Data and Methods

2.1. Sea Ice Distribution and Export

Daily estimates of sea ice concentration at a 25 × 25 km spatial resolution were downloaded from National Snow and Ice Data Center/National Oceanic and Atmospheric Administration (NOAA) (https://doi.org/10.7265/N59P2ZTG, Version 3; Peng et al., 2013). This product is a climate data record of sea ice concentration obtained from the Scanning Multichannel Microwave Radiometer onboard the Nimbus-7 satellite and the Special Sensor Microwave Imager and Imager/Sounder onboard the Defense Meteorological Satellite Program. Furthermore, in order to study the sea ice distribution at a high spatial resolution (1 km), true-color satellite imagery from the National Aeronautics and Space Administration's (NASA) Moderate Resolution Imaging Spectroradiometer (MODIS) was downloaded from the NASA Worldview application (https://worldview.earthdata.nasa.gov). These images were produced with the corrected reflectance algorithm of the NASA's Land, Atmosphere Near real-time Capability for Earth observing system that removes gross atmospheric effects, such as Rayleigh scattering, from the visible bands.

To evaluate the relationship between the sea ice concentration distribution in the Greenland Sea and the export of Arctic sea ice through Fram Strait, estimates of areal sea ice export at this strait were used. One might also consider the use of volume sea ice export; however, consistent long-term time series of volume export are not yet available (only up to 6 to 7 years, e.g., Ricker et al., 2018; Spreen et al., 2009). Monthly

mean estimates of areal sea ice export through Fram Strait were obtained from Smedsrud et al. (2017), while unpublished estimates after 2015 were furnished through the courtesy of Kjell Kloster and Stein Sandven; see also Smedsrud et al. (2011). The uncertainty associated with this monthly data set is ±5% (Smedsrud et al., 2017). In brief, the sea ice export from the Arctic Ocean was calculated across the latitude 79°N by combining sea ice concentration maps (from satellite passive-microwave observations) and ice displacement vectors. Sea ice drift vectors were derived, before February 2004, from observed monthly mean sea level pressures (from the Danish and Norwegian Meteorological Institutes, http://eklima.met.no and http://www.dmi.dk/, respectively) and after February 2004, from Synthetic Aperture Radar (SAR) satellite sensors (i.e., Envisat Advanced SAR, http://sat.nersc.no/archive; Radarsat-2, http://www.ksat.no; and Sentinel-1, https://scihub.copernicus/dhus). To recall, this present study focuses on the period 2003–2018, the era when mostly data from SAR satellite sensors are available to derive sea ice drift vectors.

2.2. Primary Production Estimates

The phytoplankton primary production (in gC m^{-2}) was estimated with a light photosynthesis model applied to satellite observations for the period 2003–2018. Our estimates are published and archived by the NOAA National Centers for Environmental Information (https://accession.nodc.noaa.gov/0208234). The model used, originally designed by Bélanger et al. (2013), is briefly described in the supporting information. The model is generally in agreement with in situ measurements and shows consistent results when used in high-latitude ocean waters (Lee et al., 2015). Water reflectance (R_{rs}) and chlorophyll-*a* concentration (Chl*a*) required for the model were downloaded from GlobColour (http://hermes. acri.fr), which provides merged observations from four satellite radiometers (SeaWiFs, MODIS Aqua, MERIS, and VIIRS) (Garver & Siegel, 1997; Maritorena et al., 2002) and produces data sets with a spatiotemporal resolution of 8 days and 25 km (~0.25°). Every pixel located in areas covered by more than 15% of sea ice concentration was discarded to avoid sea ice contamination of ocean color products (Bélanger et al., 2007). To reduce the number of missing values (i.e., due to cloud cover) in these data sets, a Data Interpolating Empirical Orthogonal Functions method (DINEOF, Alvera-Azcárate et al., 2005, 2007, 2011; Beckers & Rixen, 2003) was applied (more details in the supporting information). The DINEOF method has demonstrated effectiveness for filling spatial gaps in remote sensing datasets (see Taylor et al., 2013) and has recently been applied to phytoplankton phenology studies (e.g., Corredor-Acosta et al., 2015; Marchese et al., 2017; McGinty et al., 2016). By identifying the dominant spatial and temporal patterns, this method allows a more accurate reconstruction of missing data without any a priori statistical information (Alvera-Azcárate et al., 2005).

Finally, the required photosynthetically available radiation beneath the sea surface (Arrigo et al., 1998; Morel, 1978; Platt et al., 1980) was computed (Lee et al., 2002, 2005; Sathyendranath et al., 1989) using atmospheric observations inputs (i.e., ozone concentration, cloud fraction, and cloud optical thickness). Atmospheric data were downloaded from the Atmosphere Archive and Distribution System (https://ladsweb.modaps.eosdis.nasa.gov) with a spatiotemporal resolution of 8 days and 100 km. Prior to running the model, atmospheric observations were cropped to the study area and resampled to match the ocean color spatial resolution of 25 km. Details on the satellite-based photosynthetically available radiation algorithm and its performance can be found in Laliberté et al. (2016) and Somayajula et al. (2018).

2.3. Definition of the Phytoplankton Bloom Phenology

To study phytoplankton bloom phenology, the specific rate of change in phytoplankton biomass (r, e.g., Behrenfeld, 2010), which represents the imbalance between the phytoplankton division rate (μ, day^{-1}) and the loss rate (l, day^{-1}; that includes mortality, grazing, and sinking, i.e., $r = \mu - l$), was used. This was estimated by using the 8-day (Δt) surface Chl*a* data (as a proxy for the phytoplankton biomass) from satellite (and after the DINEOF method had been applied),

$$r = \ln(\mathrm{Chl}a_{t_1}/\mathrm{Chl}a_{t_0})/\Delta t \quad (1)$$

All annual time series of Chl*a* were smoothed with a three-point centered moving average to reduce noise. By combining phytoplankton primary production values with satellite particulate backscatter coefficient (b_{bp}) (Graff et al., 2015; Martinez-Vicente et al., 2013) data and mixed-layer depth estimates (Latarius & Quadfasel, 2016), an estimate of the springtime mixed-layer phytoplankton division rate (μ) (Behrenfeld & Boss, 2014; Mignot et al., 2018) can be obtained (supporting information).

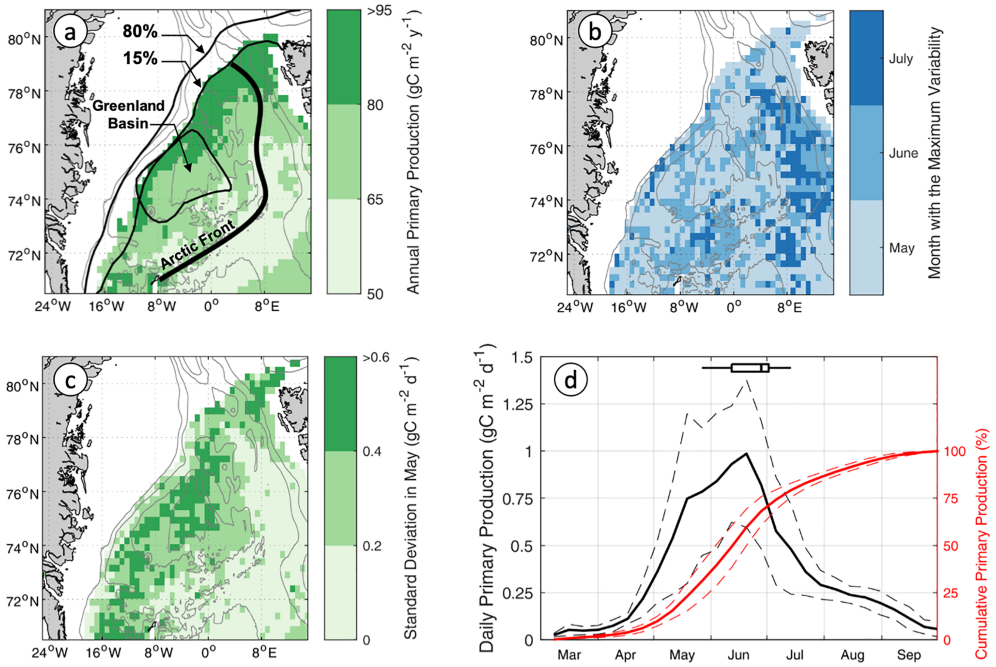

Figure 2. Primary production patterns in the Greenland Sea. (a) Climatological map of the annual primary production. Black lines represent the sea ice extent in April, based on 80% and 15% of sea ice concentration (i.e., Marginal Ice Zone) from 16 years of satellite data (2003 to 2018). The thick black line represents the location of the arctic front. (b) Climatological map of the month with the maximum standard deviation in daily primary production. (c) Climatological map of the standard deviation values of daily primary production in May. (d) Climatological annual cycle (from March to September) of primary production in the Greenland Basin (circled area in Figure 2a) with data from 2003 to 2018. Black lines represent the daily primary production and the red ones the cumulative primary production. The thick lines are the averages and the dashed ones the standard deviations. The box plot above represents the interannual variability in the date of the yearly maximum in daily primary production.

The spring bloom phenology is described by the timing of three different spring bloom phases determined by r values: the initiation (first time $r > 0$), the climax (time of the annual maximum value, r_{max}), and the termination of the biomass increase ($r = 0$, timing of the annual Chl$a$ maximum) (e.g., Llort et al., 2015).

2.4. Argo Float Data and Proxies for Water Column Stratification

Argo floats are autonomous platforms equipped with conductivity-temperature-depth (CTD) sensors to measure hydrographic profiles (salinity, temperature, and pressure) between 0 and 1,000 m every 10 days, generally. Quality controlled data measured by Argo floats within the Greenland Basin in May (circled area in Figure 2a) were downloaded from the Argo's Global Data Assembly Centers (http://doi.org/10.17882/42182) Coriolis (ftp://ftp.ifremer.fr/ifremer/argo). On average, three to four Argo float CTD profiles were available each year in May during the 2003–2018 period. Only data flagged "good" by the Argo quality control program (http://doi.org/10.13155/33951) were considered. By using the international thermodynamic equation of seawater (TEOS-10, McDougall & Barker, 2011), estimates of potential temperature (θ in °C) and density (σ in kg m^{-3}) were obtained.

To evaluate the strength of the water column stratification, two proxies derived from Argo float CTD profile data were used. The first one is the potential density gradient measured between the surface and 50 m ($\Delta\sigma_{0-50}$). The second one is the maximum value of the buoyancy (Brunt-Vaisala) frequency squared (N^2, in s^{-2}) between the surface and 50 m. Here, N^2 was determined by using the TEOS-10 expression (McDougall & Barker, 2011) that uses the vertical gradients of temperature, $N^2_T = g\alpha(\partial T/\partial z)$, and salinity, $N^2_S = g\beta(\partial S/\partial z)$, so that $N^2 = N^2_T + N^2_S$, where g is the gravity, α is the thermal expansion coefficient, β is the haline contraction coefficient, T is the conservative temperature, and S is the absolute salinity.

In addition, one biogeochemical Argo float deployed in August 2012 in the Greenland Sea provided an annual cycle of temperature, salinity, Chl*a*, nitrate concentration, and other variables for the Greenland Basin in 2013; details are provided in Mayot et al. (2018).

2.5. Air-Sea Heat Flux and Surface Wind Speed

The net air-sea heat flux was generated from the surface flux products of the fifth generation of the European Centre for Medium-Range Weather Forecasts atmospheric Re-Analysis of the global climate. Surface turbulent (sensible and latent) and radiative (net solar and thermal) heat fluxes were downloaded with a spatial resolution of 0.25° × 0.25° and a temporal resolution of 6 hr. Surface (10 m) wind speed data with the same spatiotemporal resolution were also downloaded from fifth generation of the European Centre for Medium-Range Weather Forecasts atmospheric Re-Analysis of the global climate. In order to be consistent with the temporal resolution of the primary production estimates, the heat flux and wind speed data obtained were averaged over 8 days.

3. Results

3.1. Springtime Phytoplankton Production Patterns, Exported Arctic Sea Ice, and Sea Ice Extent

Greenland Sea areas located on the western side of the polar front presented significantly higher annual primary production rates (74 [53–110] $gC{\cdot}m^{-2}{\cdot}year^{-1}$, median and interquartile range, Figure 2a) than areas located at the same range of latitude on the eastern side of the polar front (64 [56–93] $gC{\cdot}m^{-2}{\cdot}year^{-1}$; Mann-Whitney test, p value <0.001). In the Greenland Sea, the month of May presented the highest interannual variability (i.e., standard deviation with 16 years of data) in daily primary production estimates (Figure 2b). Moreover, the range of variability associated with this month was particularly high in the Greenland basins and along the Marginal Ice Zone (MIZ; >0.4 $gC{\cdot}m^{-2}{\cdot}day^{-1}$, Figure 2c). When focusing on the Greenland Basin (circled area in Figure 2a), on average, the maximum positive rate of change in primary production occurred just before 15 May (black line slope in Figure 2d), and 37% of the annual primary production had already taken place by the end of May (red line in Figure 2d). The maximal value of daily primary production was generally observed in June (box plot in Figure 2d). However, the annual peak in primary production varied from May to July, which led to a strong variability in the percentage of the annual primary production reached by the end of May: between one fourth and one half of the annual primary production (i.e., 26% to 47%, red lines in Figure 2d). Therefore, the data analysis primarily focused on understanding the variability during this key spring period (April–May).

Monthly estimates of Arctic sea ice exports through Fram Strait, from Smedsrud et al. (2017) extended to the present, and satellite estimates of sea ice concentration were used to study the relationship between exported Arctic sea ice and the sea ice distribution in the Greenland Sea. According to Smedsrud et al. (2017), the mean southward ice drift speed is ~15 ± 4 cm s^{-1} in April at the latitude of Fram Strait (79°N), which means that Arctic sea ice may reach the Greenland Sea basins (<76.5°N) in about 19 ± 5 days. Therefore, estimates of exported Arctic sea ice in April were used to study its relationship with the sea ice distribution observed in May in the Greenland Sea basins.

On average, from 2003 to 2018, the amount of Arctic sea ice exported in April through Fram Strait was $100 \times 10^3 \pm 25 \times 10^3$ km^2, and it varied between 61×10^3 and 151×10^3 km^2 (Figure 3a). The April sea ice export was lower than the average during the years 2004–20006, 2010, 2015–2016, and 2018 (Figure 3a). The mean sea ice concentration in May in the Greenland Sea basins was also lower than the average during these 7 years (−2.5 [−12 to −0.3]% anomaly) and higher than the average during the other 11 years (+1.9 [+0.2 − +9.7]% anomaly, Figure 3b), with most of the values below (above) the first quartile (third quartile) located along the continental slope. These results suggest two important points: first, a positive relationship in spring between the exported Arctic sea ice and the sea ice distribution in the Greenland Sea basins, and second, a high interannual variability in the sea ice flux and distribution.

Primary production showed significant interannual variability in spring in the Greenland Basin, with years of positive (e.g., 2007 and 2017), negative (e.g., 2006 and 2015), and neutral (e.g., 2009 and 2013) primary production anomalies (Figure 4). These spatial anomalies of spring primary production in the Greenland Basin can be examined as a function of spring sea ice export and distribution. First, the 7 years over 2004–2018 with the lowest exported Arctic sea ice in April (Figure 3a) displayed negative anomalies of spring primary

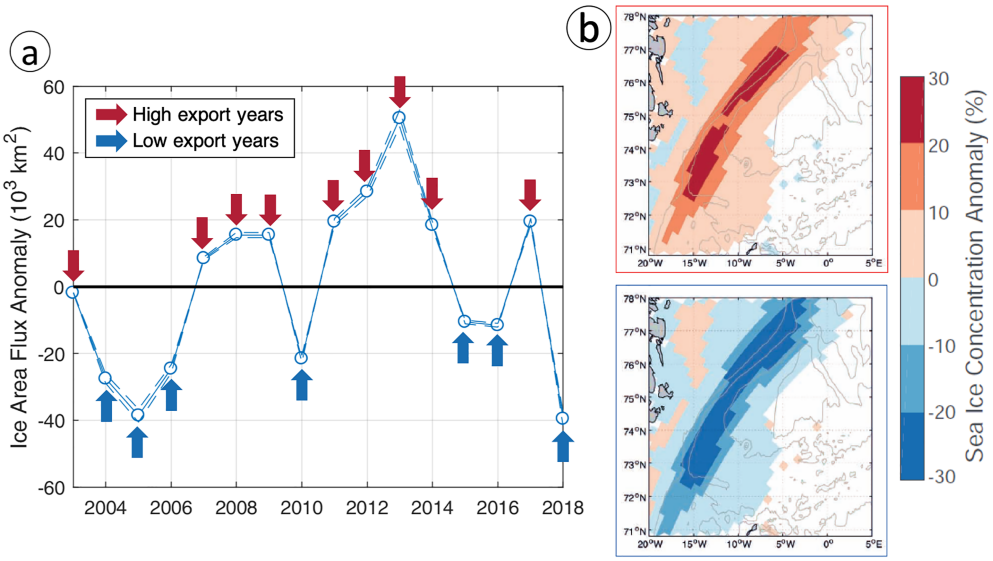

Figure 3. Relationship between the exported Arctic sea ice and the sea ice distribution in the Greenland Sea. (a) Estimates of the exported Arctic sea ice in April through Fram Strait (79°N) between 2003 and 2018. (b) Mean anomaly of the sea ice concentration in May, for the years with high (top, red arrows in Figure 3a) and low (bottom, blue arrows in Figure 3a) exported Arctic sea ice.

production in the Greenland Basin (−0.21 [−0.32 to −0.08] gC·m^{-2}·day^{-1}, Figure 4b), except for the year 2018 (Figure 4d). This exception will be separately discussed in the section 4.2. The reduced spring primary production observed during these low sea ice export years was mainly located along the MIZ and the northern part of the deep Greenland Basin (above 75°N). Second, 4 years with close (2003) or above (2007, 2011, and 2017) average exported Arctic sea ice in April (Figure 3a) was the only ones to exhibit coherent regions of positive high primary production anomalies in the Greenland Basin (+0.29 [+0.04 − +0.61] gC·m^{-2}·day^{-1}, Figure 4a). Finally, the remaining 5 years (2008, 2009, 2012, 2013, and 2014), also with above average exported Arctic sea ice (Figure 3a), displayed negative or low spring primary production anomalies (−0.07 [−0.23 to −0.09] gC·m^{-2}·d^{-1}, Figure 4c).

3.2. Springtime Water Column Stratification, Sea Ice Distribution, and Phytoplankton Bloom Phenology

Hydrographic profiles from Argo floats were used to study the stratification regime of the water column in spring in the Greenland Basin. The results presented here (Figure 5) focus on data collected in May. During years associated with positive anomalies of spring phytoplankton production patterns and above average exported Arctic sea ice, salinity profiles collected in the northern part of the deep basin (Figure 5a, data available in May 2003, 2011 and 2017) displayed low salinity values (as low as 34.23, Figure 5b) in surface layers (above 50 m). The extreme eastward extension of the sea ice extent in the Greenland Basin in spring during these years (Figure 3a) and the numerous mesoscale features observed at the ice-edge with the satellite true-color imagery (e.g., in 2011 Figure 5c top) suggest that freshwater from melted sea ice might be the cause of the measured low surface salinity. In fact, a strong stratification of the water column was observed with high median values between the surface and 50 m of potential density gradient ($\Delta\sigma$) and buoyancy frequency squared (N^2), $\Delta\sigma_{0-50} = 0.09$ kg m^{-3} (0.05–0.36 kg m^{-3}, interquartile range) and $N^2 = 7.73 \times 10^{-5}$ s^{-2} (2.73×10^{-5} – 22.18×10^{-5} s^{-2}). Moreover, 77% of the Argo float profiles collected in May in the Greenland Basin during these high ice export years showed a salinity-based stratification ($N^2_S > N^2_T$); however, most of these profiles were located in the northern part of the Greenland basin (Figure 5d top). In contrast, during years associated with negative anomalies of spring phytoplankton production patterns and low exported Arctic sea ice, salinity profiles measured in the northern deep basin (Figure 5a middle, data available in May 2006, 2015, and 2016) were mostly homogeneous from 0–200 m and the water column was weakly stratified, $\Delta\sigma_{0-50} = 0.003$ kg m^{-3} (0.003–0.008 kg m^{-3}) and $N^2 = 0.24 \times 10^{-5}$ s^{-2} (0.12×10^{-5} – 0.55×10^{-5} s^{-2}).

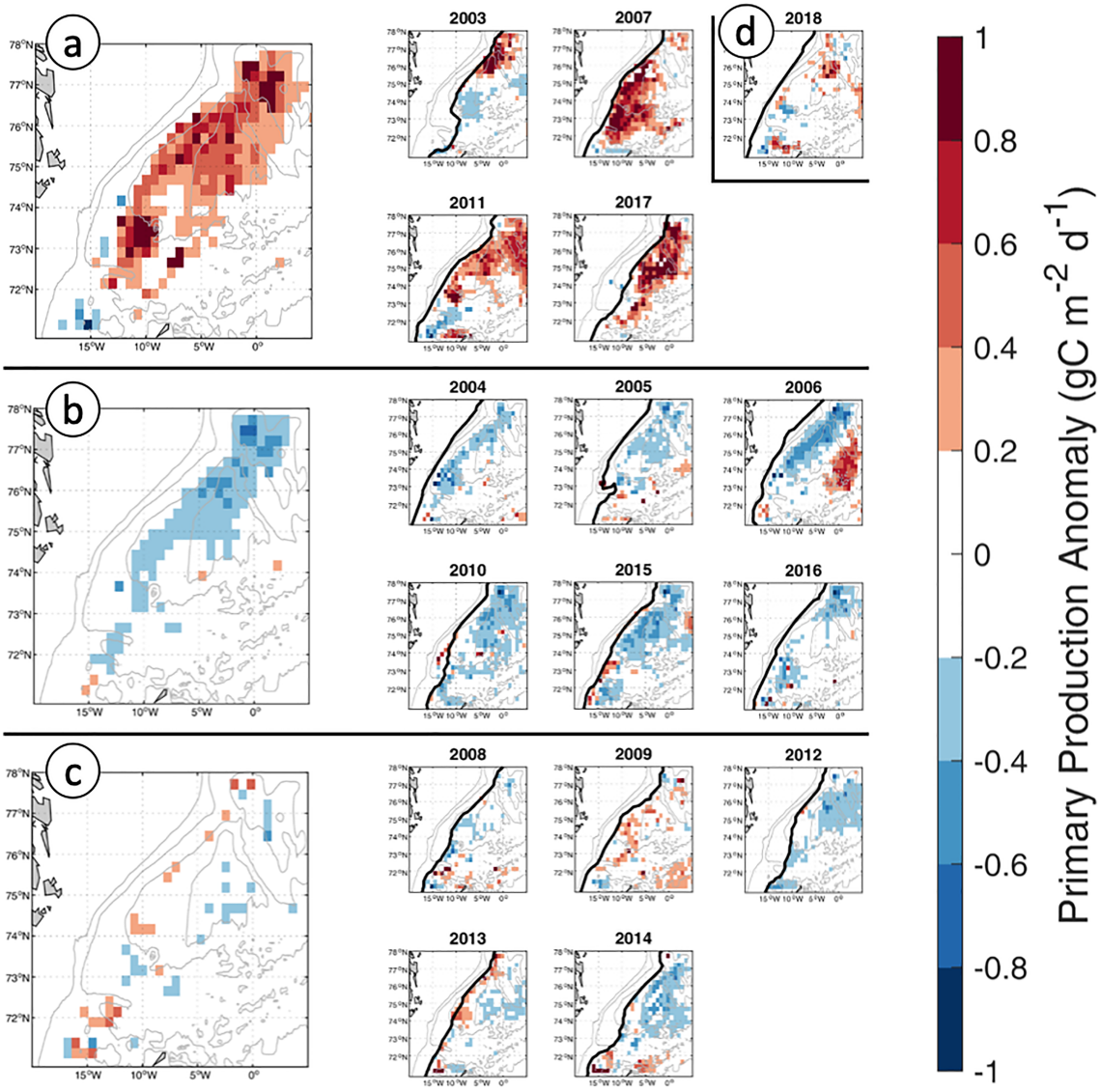

Figure 4. Anomalies of the spring (in May) primary production. The three bigger maps on the left are averages of three groups of years: (a) 2003, 2007, 2011, and 2017; (b) 2004–2006, 2010, 2015, and 2016; (c) 2008, 2009, 2012, 2013, and 2014, with the year 2018 (d) being a special case. See the text for details in the grouping. The black line in each annual map represents the location in May of the ice edge (sea ice concentration = 15%).

Even salinity profiles collected in the western part of the Greenland Basin, generally associated with the MIZ (magenta points in Figure 5a middle), were homogeneous from 0–200 m and the estimated water column stratification was low, $\Delta\sigma_{0-50} = 0.01$ kg m^{-3} (0.001–0.03 kg m^{-3}) and $N^2 = 0.57 \times 10^{-5}$ s^{-2} (0.21×10^{-5} – 1.45×10^{-5} s^{-2}). The sea ice extent barely reached this area of the Greenland Basin during these years (Figures 3 and 5c bottom), with most of the sea ice located on the continental shelf. Therefore, in May during these low ice export years and at the scale of the Greenland Basin, low N^2 values were generally observed and most of the Argo float profiles (57%) showed a temperature-based stratification ($N^2_T > N^2_S$, Figure 5d middle). In comparison, hydrographic profiles collected during the remaining years associated with above average exported Arctic sea ice but neutral anomalies of primary production (i.e., 2008, 2009, 2012, 2013, and 2014) showed a heterogeneous spatial pattern: The western part of the Greenland Basin displayed low salinity values in the surface layers and a strong water column stratification ($\Delta\sigma_{0-50} = 0.13$ kg m^{-3} [0.08–0.21] kg m^{-3}, $N^2 = 11.85 \times 10^{-5}$ s^{-2} [3.95×10^{-5} – 18.32×10^{-5}] s^{-2}; Figure 5d bottom) similar to high productive years (Figure 5d top), while the northern deep basin was characterized by homogeneous salinity

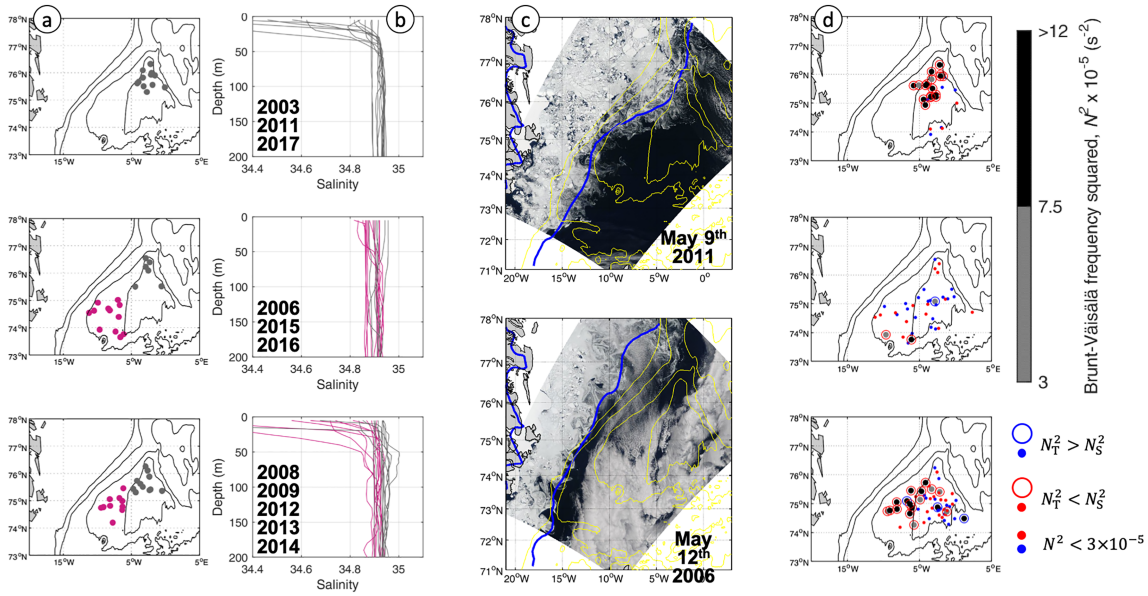

Figure 5. Relationship between springtime salinity, sea ice distribution, and the strength of the water column stratification. (a) Locations of all single salinity profiles (b) available in May between 2003 and 2018, in the northern part (gray, above 75.25°N) and western part (magenta: western basin) of the Greenland Basin and divided into three groups of years: years of positive anomalies in spring primary production (top), years of negative anomalies in spring primary production (middle), and all the other years (bottom). (c) Two MODIS corrected reflectance (True Color) images obtained in May, 2011 (top) and 2006 (bottom). The yellow lines represent the bathymetry, and the blue line represents the ice edge (sea ice concentration = 15%). (d) Maximum values of N^2 between the surface and 50 m for each Argo float profile available in the Greenland Basin. All N^2 values under 0.5×10^{-5} s^{-2} are only represented by points. The blue (red) color of the circles and points indicated that $N_T^2 > N_S^2$ ($N_T^2 < N_S^2$).

profiles and a weak water column stratification, $\Delta\sigma_{0-50} = 0.025$ kg m^{-3} (0.005–0.089 kg m^{-3}) and $N^2 = 1.62 \times 10^{-5}$ s^{-2} ($0.69\ 10^{-5}$ – 5.86×10^{-5} s^{-2}; Figure 5d bottom) similar to low productive years (Figure 5d middle). This translated into 62% of the Argo float profiles collected these years (mostly located in the western part of the Greenland Basin) presenting a salinity-based stratification ($N_S^2 > N_T^2$, Figure 5d).

Finally, observed spring anomalies in primary production appeared associated with different types of phytoplankton bloom phenology, such that both climatological means (Figures 6a and S1c) and individual annual times series (Figure S2a) of the specific rate of change in phytoplankton biomass (r, from Chl$a$ data, Figure 6a, or from b_{bp} data, Figure S1c) in the eastern deep Greenland Sea basin were different for groups of years with low versus high phytoplankton production in spring. The spring bloom initiation (first time $r \geq 0$) generally occurred in mid-April (Figure 6a). In the case of years associated with positive anomalies of spring phytoplankton production (red lines in Figure 6), the bloom initiation was followed by an early bloom climax occurring at the end of April to early May (i.e., quick and strong peak of r, with $r_{max} > 0.1$ day^{-1}) and a rapid bloom termination ($r \leq 0$) at the end of May (i.e., early decline of r). In contrast, the years associated with negative anomalies of spring phytoplankton production (blue lines in Figure 6) showed lower r values (<0.05 day^{-1}) with a bloom climax spread over a longer period, from mid-April to mid-May (i.e., $r_{max} = 0.05$ day^{-1}), and a late bloom termination at the end of June ($r \leq 0$).

4. Discussion

4.1. Springtime Exported Arctic Sea Ice and Regional Ocean Dynamics

One of the characteristics of the Greenland Sea is that its Seasonal Ice Zone and MIZ are longitudinal, with the ice edge parallel to the east Greenland coast (Figures 1 and 2a) and strongly under the influence of exported Arctic sea ice (Carmack & Wassmann, 2006). The location of the MIZ is especially important as it is the boundary between ice-covered and ice-free environments. In fact, according to the pan-Arctic oceanic typology of Carmack and Wassmann (2006), the subarctic Atlantic region is generally an α-ocean, mainly stratified by a vertical temperature gradient (i.e., $N_T^2 > N_S^2$), while the central Arctic Ocean is a β-ocean with its upper layers mainly stratified by a vertical salinity gradient (i.e., $N_T^2 < N_S^2$). However, the geographical

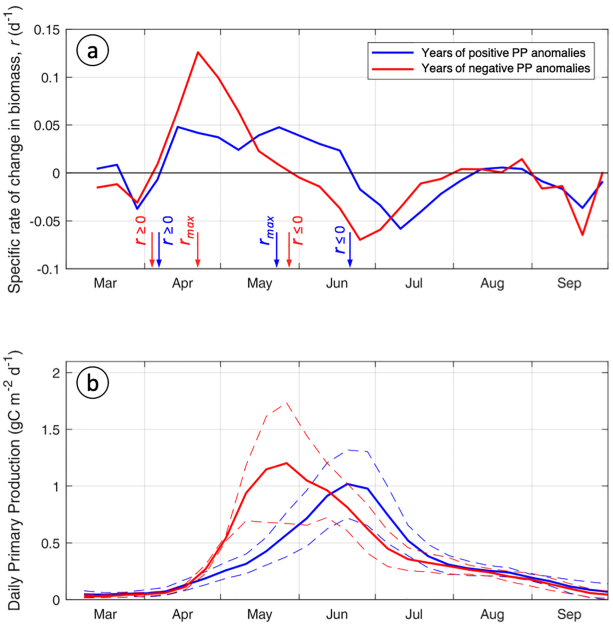

Figure 6. Climatological annual phytoplankton cycles in the deep Greenland Basin. Red line: years of positive anomalies in spring primary production, blue line: years of negative anomalies in spring primary production. (a) Climatological annual cycles of observed specific rate of change in phytoplankton biomass. The arrows represent the time of three phytoplankton spring bloom phases (i.e., initiation: $r \geq 0$, climax: r_{max}, and termination: $r \leq 0$). (b) Climatological annual cycles of primary production smoothed with a three-point centered moving average to reduce noise. The thick lines are the averages and the dashed ones the standard deviations. See Figures S2a and S2b for all individual annual time series.

boundary between these two functionally different oceanic environments is not fixed, subject to intraseasonal and interannual variabilities, like the ice edge (Carmack & Wassmann, 2006). We found that β-ocean conditions of the central Arctic Ocean extended southward along the East Greenland Current under the ice pack.

In April, the export of Arctic sea ice through Fram Strait was particularly crucial in shaping the distribution of the sea ice observed in the Greenland Sea (Figure 3). At this time of the year, the growth of sea ice is limited (Serreze & Barry, 2014) and therefore most of the sea ice present in the Greenland Basin area comes from exported Arctic Sea ice (Smedsrud et al., 2017). A major consequence is that the springtime eastward extent of the MIZ in the Greenland Basin between 2003 and 2018 was particularly limited (extensive) during years associated with low (high) exported sea ice (Figures 3 and 4). The interannual variability in spring export of Arctic sea ice (correlated with the export in April, Spearman's correlation coefficient: $r = 0.96$, p value <0.001, $n = 16$; data not shown) has been linked to the Arctic Dipole index, a measure of broader atmospheric patterns and the transpolar ice drift (Haine et al., 2015; Kwok et al., 2013; Wu et al., 2006). However, an even better predictor of Fram Strait ice export is the cross-strait sea level pressure and local wind patterns (e.g., Smedsrud et al., 2017).

In the Greenland Sea MIZ, the presence of freshwater in the surface layer is a common feature, owing to melted sea ice and Arctic Water (Carmack & Wassmann, 2006). However, most of the Arctic Water flows over the Greenland Shelf and in the East Greenland Current located over the continental slope (1,000-m bathymetry, Longhurst, 1998), as demonstrated by oxygen ratio measurements and nutrient data (de Steur et al., 2015). Thus, the freshwater signal observed in the Greenland Basin (east of the East Greenland Current) preferentially comes from locally melted sea ice (de Steur et al., 2015; Dodd et al., 2009, 2012). Therefore, during years of low exported Arctic sea ice, the freshwater content in the Greenland Basin and the springtime vertical salinity-based stratification in this area might be reduced (Figure 5), as well as the resulting springtime primary production (Figure 4; see next Section 4.2).

On the other hand, there was not a strong statistical relationship in spring between a high sea ice export through Fram Strait and a strong salinity-based water column stratification of the deep Greenland Basin. In fact, local environmental conditions at the ice edge could be decisive for the lateral advection of freshwater from melted sea ice into the deepest area of the Greenland Basin. Johannessen et al. (1992) demonstrate how, under low wind, mesoscale features at the ice edge can induce lateral transport of freshwater offshore and vertical salinity stratification in this area, especially at the bathymetric discontinuity between the Boreas and the Greenland basins. In our case, true-color imagery in early spring and during years with a detected salinity-based stratification in the deep Greenland Basin (Figures 5a–5d top) suggested the presence of such mesoscale features at the ice edge. Moreover, Germe et al. (2011) propose that the prevalence of a southerly wind along the East Greenland Coast during some winters can also induce an eastward sea ice drift (i.e., expansion of the sea ice into the Greenland Basin). Recent observations in Fram Strait further suggest that southerly winds in summer induced the eastward displacement of sea ice (Kowalczuk et al., 2019), promoting a strong salinity-based stratification and enabling the establishment of the summer deep chlorophyll maximum. In the deep Greenland Basin, the late April 2011 period, for example, was particularly subjected to southerly winds (Figure S2), which could have induced an extreme eastward transport of sea ice (Figures 4a and 5c top) and freshwater (Figure 5b top) from melted sea ice, resulting in a strong positive primary production anomaly (Figure 4a). Another year, 2013, experienced the highest springtime sea ice export at Fram Strait (Figure 3a); therefore, one might expect a strong positive primary production anomaly to follow. However, among all years with an above average springtime export of sea ice, 2013 was also the year with the strongest northerly winds during the last week of April that could compact the sea ice edge and

was ultimately associated with a neutral primary production anomaly. In summary, mesoscale features at the ice edge and wind patterns had a sufficiently strong temporal variability, from day-to-day to year-to-year (e.g., Figure S3), which could offset an above average springtime export of sea ice and thus did not coincide with a strong stratification of the deep Greenland Basin and a positive primary production anomaly (Figure 4c).

Nonetheless, during such years of above average springtime export of sea ice and only neutral to positive primary production anomalies, the sea ice extended over the continental slope (thick black lines in Figure 4c) and the western part of the Greenland Basin generally showed a strong salinity-based stratification (Figure 5d bottom). Moreover, only years with a strong springtime salinity-based stratification of the deep Greenland Basin corresponded to years with positive anomalies of springtime phytoplankton production (except 2018, discussed in the next section). However, according to the climate model projections for the Arctic, which predict a strong reduction in sea ice export through Fram Strait by the end of the 21st century (Haine et al., 2015; Vavrus et al., 2012), these years with high springtime export of sea ice and strong salinity-based stratification of the deep Greenland Basin will be less and less common.

4.2. Springtime Coupling Between Regional Physical Processes and Phytoplankton Production

According to the estimated annual cycles of specific rate of change in phytoplankton biomass (r, Figure 6a), early and late spring bloom phenologies were associated with years of positive and negative spring primary production anomalies (Figures 4a and 4b), respectively. In theory, interannual variability in the springtime stratification process may delay or advance the occurrence of bloom phases (initiation, climax, and termination) and influence the springtime phytoplankton bloom production (Llort et al., 2015). Carmack and Wassmann (2006) proposed that in the springtime MIZ, sea ice melting leaves an open ocean area that is strongly stratified by salinity, so that rapid phytoplankton biomass accumulation and production can occur until the surface nutrients are depleted. This has already been observed in situ in several Arctic seas (e.g., Barents Sea: Reigstad et al., 2002; Fram Strait: Cherkasheva et al., 2014; Smith et al., 1985). In the Greenland Sea MIZ, phytoplankton biomass accumulation can even start early under the sea ice (Mayot et al., 2018). In contrast, in subarctic Atlantic Ocean areas never covered by sea ice, the weak thermal stratification should induce a deep mixed-layer that dilutes the springtime phytoplankton biomass but ultimately may increase the nutrient availability and induce a higher integrated phytoplankton production than in seasonally sea ice covered regions (Carmack & Wassmann, 2006). We will now discuss our results within these theoretical frameworks of bloom phenology (i.e., early vs. late) and Arctic oceanic typology (β-ocean vs. α-ocean, with associated stratification, ice flux, and extent) in light of the potential consequences to the springtime phytoplankton production.

The spring bloom initiation ($r \geq 0$) occurs when the phytoplankton growth exceeds the phytoplankton losses (e.g., Sverdrup, 1953). In the Nordic Seas, phytoplankton biomass may start to accumulate in early spring and within a deep vertical mixed layer as soon as the light availability increases (e.g., Lacour et al., 2017; Mignot et al., 2016) and/or in response to a decrease in predation and nongrazing mortality rates (e.g., Banse, 1994; Behrenfeld, 2010). Focusing on the two groups of years displaying positives and negatives anomalies of spring primary production in the Greenland Sea (Figure 4), r became positive around mid-April for both groups (Figure 6a) when the heat flux switched from negative to positive (Figure S1e) which may be linked to a reduction in vertical mixing (Ferrari et al., 2015). In situ data from a biogeochemical Argo float that measured the vertical distribution of the Chl*a* in the deep Greenland Basin over the year 2013 (Figure S3, Mayot et al., 2018) also suggested that r, estimated from vertically integrated Chl*a* in the mixed layer, became positive when the heat flux switched from negative to positive. Despite the ecological significance of the bloom onset (thoroughly discussed for the Nordic Seas by Mignot et al., 2016), the primary production level in the Greenland Basin between the bloom onset and climax remained low (<0.5 gC·m^{-2}·day^{-1}, Figure 6b).

The primary production significantly increased between the following bloom climax (r_{max}) and termination ($r \leq 0$) phases (ranging 0.5–1.40 gC·m^{-2}·day^{-1}, Figure 6), which should correspond, in theory, to the time of the year with the highest growth rate for the phytoplankton population (e.g., Behrenfeld et al., 2016). In the Greenland Basin, because the bloom onset had a low interannual variability (Figure 6a), the timing of these latter two phases (i.e., climax and termination) could be better used to describe the bloom phenology as early or late. Theoretically, in the case of an early bloom there would be an early bloom climax and termination

(i.e., an early r_{max} followed by a sudden drop in r, Llort et al., 2015). This framework matches the phytoplankton bloom characteristics assigned to the theoretical β-ocean environment of Carmack and Wassmann (2006). In view of the annual cycles of r associated with the springtime primary production anomalies observed (Figures 6a and S1c), years associated with positive (negative) anomalies of spring primary production displayed an early (delayed) bloom phenology.

The stratification process influences the predator-prey interactions and the light-mixing regime that have long been considered the primary drivers of the bloom phenology and the subject of much discussion (e.g., from Sverdrup, 1953 to Llort et al., 2015; Janout et al., 2016 and Lowry et al., 2018 for the Arctic). In our case, years associated with strong springtime salinity-based stratification of the Greenland Basin, which correspond to β-type oceans with high sea ice flux and extent, could be related to an early bloom and a high primary production level in May. In this case, the springtime strong vertical stratification of the surface layers probably provided the optimal growth conditions to the phytoplankton cells to consume the available nutrients, thus inducing early bloom climax and termination phases. The availability of nutrients at the bloom climax in the deep Greenland Basin was supported by the biogeochemical Argo float measurements in 2013 (Figure S4b), with around 12 μmol kg^{-1} of nitrate available at the time of the bloom climax.

At the pan-Arctic scale, the interannual variability in sea ice extent (or ice-free area) influences the interannual variability in total annual Arctic phytoplankton production (without considering the under-ice phytoplankton production, e.g., Arrigo et al., 2008; Arrigo & van Dijken, 2015), with the nutrient availability setting an upper limit for the overall values reached (e.g., Codispoti et al., 2013; Tremblay et al., 2015). Regarding the interannual variability in the seasonal pan-Arctic phytoplankton biomass, Behrenfeld et al. (2016) suggest that the variability in mixed layer growth conditions has a stronger influence than the variability in sea ice extent (as opposed to its influence on an annual scale). However, in our case and at the regional scale of the Greenland Sea, it was possible to detect an influence of the interannual variability in seasonal sea ice flux and extent on the seasonal stratification regime (influencing the mixed layer growth conditions) and on a seasonal ecological event, such as the phytoplankton spring bloom. Behrenfeld et al. (2016) analysis, carried over the whole pan-Arctic, probably does not hold when focusing at regional scales. Results here further highlighted the particularity of the Greenland Sea, compared to the rest of the pan-Arctic, of being strongly influenced by the export of Arctic sea ice. It also emphasized the ecological link that exists between the Arctic Ocean and the subarctic Atlantic Ocean. In contrast to the Labrador Sea, where the annual cycle of phytoplankton biomass has been related to the advection of freshwater originating from both the Arctic Ocean and the Greenland ice sheet runoff (e.g., Lacour et al., 2015), the phytoplankton production in the Greenland Sea is under the influence of sea ice discharge through Fram Strait.

The year 2018 showed low export of Arctic sea ice in April with a subsequent low sea ice extent in May (Figures 3a and 4d), usually associated with an α-type ocean, but the springtime phytoplankton production anomaly in the Greenland Basin was neutral and even positive in its deeper northern part (Figure 4d). Although a weak temperature-based stratification would be expected due to the observed low sea ice conditions, the spring-summer temperatures in the pan-Arctic area in 2018 were exceptionally warm; for example, May 2018 set a record, being the warmest May of all regular Svalbard meteorological stations since 1898 (surface air temperature, Osborne et al., 2018). In the Greenland Basin, the heat flux was particularly intense, reaching 118 W m^{-2} in early May, the highest value recorded between 2003 and 2018 (Figure S2ee). The temperature-based stratification may have thus been particularly strong and could have driven an early bloom and higher spring primary production in May in the Greenland Basin. During this exceptionally warm year, the phytoplankton bloom phenology and production manifested characteristics normally associated with β-ocean environments, rather than the ones expected for α-type ocean in this region at this time of the year. The frequency of such exceptionally warm years will probably increase (Collins et al., 2019), while the export of sea ice will decrease and the export of freshwater increase (Haine et al., 2015; Vavrus et al., 2012). Assuming that Arctic water remains within the East Greenland Current as at present (Dodd et al., 2009, 2012), such changes could induce the Greenland Sea, east of the East Greenland Current, to become only an α-type ocean with an early phytoplankton bloom. However, such stronger warming events of the Greenland Sea and the predicted increase in liquid freshwater export may have other unexpected consequences, not assessed in this study, on the planktonic ecosystem structure (e.g., shift in plankton

communities) and biogeochemical processes in this North Atlantic transition zone (e.g., Carmack et al., 2016; Carmack & Wassmann, 2006; Engel et al., 2019).

5. Conclusions

Results from this study provided evidences that Fram Strait sea ice outflow, by affecting the water column stability, influenced the phytoplankton production in the Greenland Sea. Overall, a high springtime Arctic ice export through Fram Strait can lead to a strong salinity-based stratification and an early phytoplankton bloom in the Greenland Basin. On the contrary, in case of a reduction in ice export, as climate models predict, a weak water column stratification of the Greenland Basin led to delayed phytoplankton spring blooms. Such variability in the phytoplankton bloom occurrence, driven by the Arctic ice flux, may have substantial consequences on the timing and quantity of biological carbon export and the production of higher trophic levels. Furthermore, the unexpected results associated with the exceptional warm year 2018 (i.e., a year with low ice export but an early phytoplankton bloom driven by thermal stratification) demonstrated the nonlinearity between the ice export through Fram Strait and the phytoplankton bloom timing in the Greenland Sea. Summing up, these findings clearly show how phytoplankton phenology and production in the subarctic Atlantic (above 55°N) can be strongly influenced by the ongoing changes in the Arctic Ocean. In view of this, the subarctic Atlantic appears as a crucial transitional area (i.e., connecting the Arctic and Atlantic Oceans) where continuing to investigate key physical and biogeochemical processes influencing the pelagic environment will reveal potential future ecosystem shifts in response to climate change.

Acknowledgments
We thank Lars Smedstrud, Kjell Kloster, and Stein Sandven for providing sea ice flux data. We are grateful to NASA and NSIDC/NOAA for open access to their remotely sensed products. Argo data were collected and made freely available by the International Argo Program and the national programs that contribute to it (http://www.argo.ucsd.edu, http://argo.jcommops.org). The Argo Program is part of the Global Ocean Observing System. To generate the net air-sea heat flux and surface wind speed maps, data from ERA5 were downloaded from the Copernicus Climate Change Service Climate Data Store (CDS), in December 2018 (https://cds.climate.copernicus.eu/cdsapp#!/dataset/reanalysis-era5-single-levels?tab=overview). Primary production estimates are freely available and published by the NOAA National Centers for Environmental Information (https://accession.nodc.noaa.gov/0208234). This work was funded by NASA NNX17AB99G/80NSSC8K0081 to P. A. M. M. Steele would like to acknowledge the support of NSF through Grant PLR-1503298 and NOAA through Grant NA15OAR4320063.

References

Alvera-Azcárate, A., Barth, A., Beckers, J. M., & Weisberg, R. H. (2007). Multivariate reconstruction of missing data in sea surface temperature, chlorophyll, and wind satellite fields. *Journal of Geophysical Research*, *112*, C03008. https://doi.org/10.1029/2006JC003660

Alvera-Azcárate, A., Barth, A., Rixen, M., & Beckers, J. M. (2005). Reconstruction of incomplete oceanographic data sets using empirical orthogonal functions: Application to the Adriatic Sea surface temperature. *Ocean Modelling*, *9*(4), 325–346. https://doi.org/10.1016/j.ocemod.2004.08.001

Alvera-Azcárate, A., Barth, A., Sirjacobs, D., Lenartz, F., & Beckers, J. M. (2011). Data interpolating empirical orthogonal functions (DINEOF): A tool for geophysical data analyses. *Mediterranean Marine Science*, *12*(3), 5–11. https://doi.org/10.12681/mms.64

Ardyna, M., Babin, M., Gosselin, M., Devred, E., Bélanger, S., Matsuoka, A., & Tremblay, J. E. (2013). Parameterization of vertical chlorophyll *a* in the Arctic Ocean: Impact of the subsurface chlorophyll maximum on regional, seasonal, and annual primary production estimates. *Biogeosciences*, *10*(6), 4383–4404. https://doi.org/10.5194/bg-10-4383-2013

Ardyna, M., Babin, M., Gosselin, M., Devred, E., Rainville, L., & Tremblay, J. É. (2014). Recent Arctic Ocean sea ice loss triggers novel fall phytoplankton blooms. *Geophysical Research Letters*, *41*, 6207–6212. https://doi.org/10.1002/2014GL061047

Arrigo, K. R., van Dijken, G., & Pabi, S. (2008). Impact of a shrinking Arctic ice cover on marine primary production. *Geophysical Research Letters*, *35*, L19603. https://doi.org/10.1029/2008GL035028

Arrigo, K. R., & van Dijken, G. L. (2015). Continued increases in Arctic Ocean primary production. *Progress in Oceanography*, *136*, 60–70. https://doi.org/10.1016/j.pocean.2015.05.002

Arrigo, K. R., van Dijken, G. L., Castelao, R. M., Luo, H., Rennermalm, Å. K., Tedesco, M., et al. (2017). Melting glaciers stimulate large summer phytoplankton blooms in southwest Greenland waters. *Geophysical Research Letters*, *44*, 6278–6285. https://doi.org/10.1002/2017GL073583

Arrigo, K. R., Worthen, D., Schnell, A., & Lizotte, M. P. (1998). Primary production in Southern Ocean waters. *Journal of Geophysical Research*, *103*(C8), 15,587–15,600. https://doi.org/10.1029/98JC00930

Arzel, O., Fichefet, T., Goosse, H., & Dufresne, J. L. (2008). Causes and impacts of changes in the Arctic freshwater budget during the twentieth and twenty-first centuries in an AOGCM. *Climate Dynamics*, *30*(1), 37–58. https://doi.org/10.1007/s00382-007-0258-5

Banse, K. (1994). Grazing and zooplankton production as key controls of phytoplankton production in the open ocean. *Oceanography*, *7*(1), 13–20.

Beckers, J. M., & Rixen, M. (2003). EOF calculations and data filling from incomplete oceanographic datasets. *Journal of Atmospheric and Oceanic Technology*, *20*(12), 1839–1856. https://doi.org/10.1175/1520-0426(2003)020<1839:ECADFF>2.0.CO;2

Behrenfeld, M. J. (2010). Abandoning Sverdrup's critical depth hypothesis on phytoplankton blooms. *Ecology*, *91*(4), 977–989.

Behrenfeld, M. J., & Boss, E. S. (2014). Resurrecting the ecological underpinnings of ocean plankton blooms. *Annual Review of Marine Science*, *6*(1), 167–194. https://doi.org/doi:10.1146/annurev-marine-052913-021325

Behrenfeld, M. J., Hu, Y., O'Malley, R. T., Boss, E. S., Hostetler, C. A., Siegel, D. A., et al. (2016). Annual boom–bust cycles of polar phytoplankton biomass revealed by space-based lidar. *Nature Geoscience*, *10*(2), 118–122. https://doi.org/10.1038/ngeo2861

Bélanger, S., Babin, M., & Tremblay, J.-É. (2013). Increasing cloudiness in Arctic damps the increase in phytoplankton primary production due to sea ice receding. *Biogeosciences*, *10*(6), 4087–4101. https://doi.org/10.5194/bg-10-4087-2013

Bélanger, S., Ehn, J. K., & Babin, M. (2007). Impact of sea ice on the retrieval of water-leaving reflectance, chlorophyll a concentration and inherent optical properties from satellite ocean color data. *Remote Sensing of Environment*, *111*(1), 51–68. https://doi.org/10.1016/j.rse.2007.03.013

Brakstad, A., Våge, K., Håvik, L., & Moore, G. W. K. (2018). Water mass transformation in the Greenland Sea during the period 1986–2016. *Journal of Physical Oceanography*, *49*(1), 121–140. https://doi.org/10.1175/jpo-d-17-0273.1

Carmack, E., & Wassmann, P. (2006). Food webs and physical-biological coupling on pan-Arctic shelves: Unifying concepts and comprehensive perspectives. *Progress in Oceanography*, *71*(2–4), 446–477. https://doi.org/10.1016/j.pocean.2006.10.004

Carmack, E. C., Yamamoto-Kawai, M., Haine, T. W. N., Bacon, S., Bluhm, B. A., Lique, C., et al. (2016). Freshwater and its role in the Arctic Marine System: Sources, disposition, storage, export, and physical and biogeochemical consequences in the Arctic and global oceans. *Journal of Geophysical Research: Biogeosciences*, *121*, 675–717. https://doi.org/10.1002/2015JG003140

Cherkasheva, A., Bracher, A., Melsheimer, C., Köberle, C., Gerdes, R., Nöthig, E. M., et al. (2014). Influence of the physical environment on polar phytoplankton blooms: A case study in the Fram Strait. *Journal of Marine Systems*, *132*, 196–207. https://doi.org/10.1016/j.jmarsys.2013.11.008

Codispoti, L. A., Kelly, V., Thessen, A., Matrai, P., Suttles, S., Hill, V., et al. (2013). Synthesis of primary production in the Arctic Ocean: III. Nitrate and phosphate based estimates of net community production. *Progress in Oceanography*, *110*, 126–150. https://doi.org/10.1016/j.pocean.2012.11.006

Collins, M., Sutherland, M., Bouwer, L., Cheong, S., Frölicher, T., Des Combes, H. J., et al. (2019). Extremes, abrupt changes and managing risks. In H. Pörtner, D. C. Roberts, V. Masson-Delmotte, P. Zhai, M. Tignor, E. Poloczanska, et al. (Eds.), IPCC Special Report on the Ocean and Cryosphere in a Changing Climate (pp. 6–1 6–94). Retrieved from https://report.ipcc.ch/srocc/pdf/SROCC_FinalDraft_Chapter6.pdf.

Comiso, J. C., Wadhams, P., Pedersen, L. T., & Gersten, R. A. (2001). Seasonal and interannual variability of the Odden ice tongue and a study of environmental effects. *Journal of Geophysical Research*, *106*(C5), 9093–9116. https://doi.org/10.1029/2000JC000204

Corredor-Acosta, A., Morales, C. E., Hormazabal, S., Andrade, I., & Correa-Ramirez, M. A. (2015). Phytoplankton phenology in the coastal upwelling region off central-southern Chile (35°S-38°S): Time-space variability, coupling to environmental factors, and sources of uncertainty in the estimates. *Journal of Geophysical Research: Oceans*, *120*, 813–831. https://doi.org/10.1002/2014JC010330

de Steur, L., Pickart, R. S., Torres, D. J., & Valdimarsson, H. (2015). Recent changes in the freshwater composition east of Greenland. *Geophysical Research Letters*, *42*, 2326–2332. https://doi.org/10.1002/2014GL062759

Dodd, P. A., Heywood, K. J., Meredith, M. P., Naveira-Garabato, A. C., Marca, A. D., & Falkner, K. K. (2009). Sources and fate of freshwater exported in the East Greenland Current. *Geophysical Research Letters*, *36*, L19608. https://doi.org/10.1029/2009GL039663

Dodd, P. A., Rabe, B., Hansen, E., Falck, E., Mackensen, A., Rohling, E., et al. (2012). The freshwater composition of the Fram Strait outflow derived from a decade of tracer measurements. *Journal of Geophysical Research*, *117*, C11005. https://doi.org/10.1029/2012JC008011

Engel, A., Bracher, A., Dinter, T., Endres, S., Grosse, J., Metfies, K., et al. (2019). Inter-annual variability of organic carbon concentrations in the eastern Fram Strait during summer (2009–2017). *Frontiers in Marine Science*, *6*, 187. https://doi.org/10.3389/FMARS.2019.00187

Ferrari, R., Merrifield, S. T., & Taylor, J. R. (2015). Shutdown of convection triggers increase of surface chlorophyll. *Journal of Marine Systems*, *147*, 116–122.

Frajka-Williams, E., & Rhines, P. B. (2010). Physical controls and interannual variability of the Labrador Sea spring phytoplankton bloom in distinct regions. *Deep Sea Research Part I: Oceanographic Research Papers*, *57*(4), 541–552.

Garver, S. A., & Siegel, D. A. (1997). Inherent optical property inversion of ocean color spectra and its biogeochemical interpretation: 1. Time series from the Sargasso Sea. *Journal of Geophysical Research*, *102*(C8), 18,607–18,625. https://doi.org/10.1029/96JC03243

Germe, A., Houssais, M. N., Herbaut, C., & Cassou, C. (2011). Greenland Sea sea ice variability over 1979–2007 and its link to the surface atmosphere. *Journal of Geophysical Research*, *116*, C10034. https://doi.org/10.1029/2011JC006960

Gradinger, R. (1995). Climate change and biological oceanography of the Arctic Ocean. *Philosophical Transactions of the Royal Society of London A*, *352*(1699), 277–286. https://doi.org/10.1098/rsta.1995.0070

Graff, J. R., Westberry, T. K., Milligan, A. J., Brown, M. B., Dall'Olmo, G., Dongen-Vogels, V., et al. (2015). Analytical phytoplankton carbon measurements spanning diverse ecosystems. *Deep Sea Research Part I: Oceanographic Research Papers*, *102*, 16–25. https://doi.org/10.1016/J.DSR.2015.04.006

Greene, C. H., & Pershing, A. J. (2007). Climate drives sea change. *Science*, *315*(5815), 1084–1085. https://doi.org/10.1126/science.1136495

Haine, T. W. N., Curry, B., Gerdes, R., Hansen, E., Karcher, M., Lee, C., et al. (2015). Arctic freshwater export: Status, mechanisms, and prospects. *Global and Planetary Change*, *125*, 13–35. https://doi.org/10.1016/j.gloplacha.2014.11.013

Harrison, W. G., Børsheim, K. Y., Li, W. K., Maillet, G. L., Pepin, P., Sakshaug, E., et al. (2013). Phytoplankton production and growth regulation in the Subarctic North Atlantic: A comparative study of the Labrador Sea-Labrador/Newfoundland shelves and Barents/Norwegian/Greenland seas and shelves. *Progress in Oceanography*, *114*, 26–45. https://doi.org/10.1016/j.pocean.2013.05.003

Horvat, C., Jones, D. R., Iams, S., Schroeder, D., Flocco, D., & Feltham, D. (2017). The frequency and extent of sub-ice phytoplankton blooms in the Arctic Ocean. *Science Advances*, *3*(3), e1601191. https://doi.org/10.1126/sciadv.1601191

Jahn, A., & Holland, M. M. (2013). Implications of Arctic sea ice changes for North Atlantic deep convection and the meridional overturning circulation in CCSM4-CMIP5 simulations. *Geophysical Research Letters*, *40*, 1206–1211. https://doi.org/10.1002/grl.50183

Janout, M. A., Hölemann, J., Waite, A. M., Krumpen, T., von Appen, W. J., & Martynov, F. (2016). Sea-ice retreat controls timing of summer plankton blooms in the Eastern Arctic Ocean. *Geophysical Research Letters*, *43*, 12,493–12,501. https://doi.org/10.1002/2016GL071232

Johannessen, O. M., Campbell, W. J., Shuchman, R., Sandven, S., Gloersen, P., Johannessen, J. A., et al. (1992). In F. D. Carsey (Ed.), *Microwave study programs of air–ice–ocean interactive processes in the seasonal ice zone of the Greenland and Barents Seas*, Geophysical Monograph Series (Vol. *68*, pp. 261–290). Washington, DC: American Geophysical Union. https://doi.org/10.1029/gm068p0261

Joli, N., Gosselin, M., Ardyna, M., Babin, M., Onda, D. F., Tremblay, J. É., & Lovejoy, C. (2018). Need for focus on microbial species following ice melt and changing freshwater regimes in a Janus Arctic Gateway. *Scientific Reports*, *8*(1), 9405. https://doi.org/10.1038/s41598-018-27705-6

Kahru, M., Brotas, V., Manzano-Sarabia, M., & Mitchell, B. G. (2011). Are phytoplankton blooms occurring earlier in the Arctic? *Global Change Biology*, *17*(4), 1733–1739. https://doi.org/10.1111/j.1365-2486.2010.02312.x

Kahru, M., Lee, Z., Mitchell, B. G., & Nevison, C. D. (2016). Effects of sea ice cover on satellite-detected primary production in the Arctic Ocean. *Biology Letters*, *12*(11), 20160223. https://doi.org/10.1098/rsbl.2016.0223

Kowalczuk, P., Sagan, S., Makarewicz, A., Meler, J., Borzycka, K., Zabłocka, M., et al. (2019). Bio-optical properties of surface waters in the Atlantic Water inflow region off Spitsbergen (Arctic Ocean). *Journal of Geophysical Research: Oceans*, *124*, 1964–1987. https://doi.org/10.1029/2018JC014529

Kwok, R., Cunningham, G. F., & Pang, S. S. (2004). Fram Strait sea ice outflow. *Journal of Geophysical Research*, *109*, C01009. https://doi.org/10.1029/2003JC001785

Kwok, R., Spreen, G., & Pang, S. (2013). Arctic sea ice circulation and drift speed: Decadal trends and ocean currents. *Journal of Geophysical Research: Oceans*, *118*, 2408–2425. https://doi.org/10.1002/jgrc.20191

Lacour, L., Ardyna, M., Stec, K. F., Claustre, H., Prieur, L., Poteau, A., et al. (2017). Unexpected winter phytoplankton blooms in the North Atlantic subpolar gyre. *Nature Geoscience*, *10*(11), 836–839. https://doi.org/10.1038/ngeo3035

Lacour, L., Claustre, H., Prieur, L., & D'Ortenzio, F. (2015). Phytoplankton biomass cycles in the North Atlantic subpolar gyre: A similar mechanism for two different blooms in the Labrador Sea. *Geophysical Research Letters*, *42*, 5403–5410. https://doi.org/10.1002/2015GL064540

Laliberté, J., Bélanger, S., & Frouin, R. (2016). Evaluation of satellite-based algorithms to estimate photosynthetically available radiation (PAR) reaching the ocean surface at high northern latitudes. *Remote Sensing of Environment*, *184*, 199–211. https://doi.org/10.1016/j.rse.2016.06.014

Latarius, K., & Quadfasel, D. (2010). Seasonal to inter-annual variability of temperature and salinity in the Greenland Sea Gyre: Heat and freshwater budgets. *Tellus Series A: Dynamic Meteorology and Oceanography*, *62*(4), 497–515. https://doi.org/10.1111/j.1600-0870.2010.00453.x

Latarius, K., & Quadfasel, D. (2016). Water mass transformation in the deep basins of the Nordic Seas: Analyses of heat and freshwater budgets. *Deep Sea Research Part I: Oceanographic Research Papers*, *114*, 23–42. https://doi.org/10.1016/j.dsr.2016.04.012

Lee, Y. J., Matrai, P. A., Friedrichs, M. A. M., Saba, V. S., Antoine, D., Ardyna, M., et al. (2015). An assessment of phytoplankton primary productivity in the Arctic Ocean from satellite ocean color/in situ chlorophyll-a based models. *Journal of Geophysical Research: Oceans*, *120*, 6508–6541. https://doi.org/10.1002/2015JC011018

Lee, Z. P., Carder, K. L., & Arnone, R. A. (2002). Deriving inherent optical properties from water color: A multiband quasi-analytical algorithm for optically deep waters. *Applied Optics*, *41*(27), 5755. https://doi.org/10.1364/AO.41.005755

Lee, Z. P., Du, K. P., & Arnone, R. (2005). A model for the diffuse attenuation coefficient of downwelling irradiance. *Journal of Geophysical Research*, *110*, C02016. https://doi.org/10.1029/2004JC002275

Llort, J., Lévy, M., Sallée, J. B., & Tagliabue, A. (2015). Onset, intensification, and decline of phytoplankton blooms in the Southern Ocean. *ICES Journal of Marine Science*, *72*(6), 1971–1984. https://doi.org/10.1093/icesjms/fsv053

Longhurst, A. (1998). *Ecological Geography of the Sea*. San Diego: Academic Press.

Lowry, K. E., Pickart, R. S., Selz, V., Mills, M. M., Pacini, A., Lewis, K. M., et al. (2018). Under-ice phytoplankton blooms inhibited by spring convective mixing in refreezing leads. *Journal of Geophysical Research: Oceans*, *123*, 90–109. https://doi.org/10.1002/2016JC012575

Macias-Fauria, M., & Post, E. (2018). Effects of sea ice on Arctic biota: An emerging crisis discipline. *Biology Letters*, *14*(3), 20170702. https://doi.org/10.1098/RSBL.2017.0702

Marchese, C., Albouy, C., Tremblay, J. É., Dumont, D., D'Ortenzio, F., Vissault, S., & Bélanger, S. (2017). Changes in phytoplankton bloom phenology over the North Water (NOW) polynya: A response to changing environmental conditions. *Polar Biology*, *40*(9), 1721–1737. https://doi.org/10.1007/s00300-017-2095-2

Marchese, C., Castro de la Guardia, L., Myers, P. G., & Bélanger, S. (2019). Regional differences and inter-annual variability in the timing of surface phytoplankton blooms in the Labrador Sea. *Ecological Indicators*, *96*, 81–90. https://doi.org/10.1016/j.ecolind.2018.08.053

Maritorena, S., Siegel, D. A., & Peterson, A. R. (2002). Optimization of a semianalytical ocean color model for global-scale applications. *Applied Optics*, *41*(15), 2705–2714. https://doi.org/10.1364/AO.41.002705

Martinez-Vicente, V., Dall'Olmo, G., Tarran, G., Boss, E., & Sathyendranath, S. (2013). Optical backscattering is correlated with phytoplankton carbon across the Atlantic Ocean. *Geophysical Research Letters*, *40*, 1154–1158. https://doi.org/10.1002/grl.50252

Mayot, N., Matrai, P., Ellingsen, I. H., Steele, M., Johnson, K., Riser, S. C., & Swift, D. (2018). Assessing phytoplankton activities in the seasonal ice zone of the Greenland Sea over an annual cycle. *Journal of Geophysical Research: Oceans*, *123*, 8004–8025. https://doi.org/10.1029/2018JC014271

McDougall, T. J., & Barker, P. M. (2011). Getting started with TEOS-10 and the Gibbs Seawater (GSW) oceanographic toolbox. Scor/Iapso Wg127, 28. https://doi.org/SCOR/IAPSO WG127

McGinty, N., Guðmundsson, K., Ágústsdóttir, K., & Marteinsdóttir, G. (2016). Environmental and climactic effects of chlorophyll-a variability around Iceland using reconstructed satellite data fields. *Journal of Marine Systems*, *163*, 31–42. https://doi.org/10.1016/j.jmarsys.2016.06.005

Meredith, M., Sommerkorn, M., Cassotta, S., Derksen, D., Ekaykin, A., Hollowed, A., et al. (2019). Polar Regions. In H. Pörtner, D. C. Roberts, V. Masson-Delmotte, P. Zhai, M. Tignor, E. Poloczanska, et al. (Eds.), IPCC Special Report on the Ocean and Cryosphere in a Changing Climate (pp. 3–1 3–173). Retrieved from https://report.ipcc.ch/srocc/pdf/SROCC_FinalDraft_Chapter3.pdf.

Mignot, A., Ferrari, R., & Arne Mork, K. (2016). Spring bloom onset in the Nordic Seas. *Biogeosciences*, *13*(11), 3485–3502. https://doi.org/10.5194/bg-13-3485-2016

Mignot, A., Ferrari, R., & Claustre, H. (2018). Floats with bio-optical sensors reveal what processes trigger the North Atlantic bloom. *Nature Communications*, *9*(1), 190. https://doi.org/10.1038/s41467-017-02143-6

Morel, A. (1978). Available, usable, and stored radiant energy in relation to marine photosynthesis. *Deep-Sea Research*, *25*(8), 673–688. https://doi.org/10.1016/0146-6291(78)90623-9

Morel, A. (1991). Light and marine photosynthesis: A spectral model with geochemical and climatological implications. *Progress in Oceanography*, *26*(3), 263–306. https://doi.org/10.1016/0079-6611(91)90004-6

Osborne, E., Richter-Menge, J., & Jeffries, M. (2018). Arctic report card 2018. Retrieved from https://www.arctic.noaa.gov/Report-Card

Osman, M. B., Das, S. B., Trusel, L. D., Evans, M. J., Fischer, H., Grieman, M. M., et al. (2019). Industrial-era decline in subarctic Atlantic productivity. *Nature*, *569*(7757), 551–555. https://doi.org/10.1038/s41586-019-1181-8

Pabi, S., van Dijken, G. L., & Arrigo, K. R. (2008). Primary production in the Arctic Ocean, 1998–2006. *Journal of Geophysical Research*, *113*, C08005. https://doi.org/10.1029/2007JC004578

Peng, G., Meier, W. N., Scott, D. J., & Savoie, M. H. (2013). A long-term and reproducible passive microwave sea ice concentration data record for climate studies and monitoring. *Earth System Science Data*, *5*(2), 311–318. https://doi.org/10.5194/essd-5-311-2013

Platt, T., Gallegos, C. L., & Harrison, W. G. (1980). Photoinhibition of photosynthesis in natural assemblages of marine phytoplankton. *Journal of Marine Research*, *38*, 687–701.

Reigstad, M., Wassmann, P., Wexels Riser, C., Øygarden, S., & Rey, F. (2002). Variations in hydrography, nutrients and chlorophyll a in the marginal ice-zone and the central Barents Sea. *Journal of Marine Systems*, *38*(1–2), 9–29. https://doi.org/10.1016/S0924-7963(02)00167-7

Renaut, S., Devred, E., & Babin, M. (2018). Northward expansion and intensification of phytoplankton growth during the early ice-free season in Arctic. *Geophysical Research Letters*, *45*, 10,590–10,598. https://doi.org/10.1029/2018GL078995

Ricker, R., Girard-Ardhuin, F., Krumpen, T., & Lique, C. (2018). Satellite-derived sea ice export and its impact on Arctic ice mass balance. *The Cryosphere*, *12*(9), 3017–3032. https://doi.org/10.5194/tc-12-3017-2018

Sakshaug, E. (2004). Primary and secondary production in the Arctic seas. In *The organic carbon cycle in the Arctic Ocean*, (pp. 57–81). Berlin, Heidelberg: Springer Berlin Heidelberg. https://doi.org/10.1007/978-3-642-18912-8_3

Sathyendranath, S., Platt, T., Caverhill, C. M., Warnock, R. E., & Lewis, M. R. (1989). Remote sensing of oceanic primary production: Computations using a spectral model. *Deep Sea Research Part A, Oceanographic Research Papers*, *36*(3), 431–453. https://doi.org/10.1016/0198-0149(89)90046-0

Serreze, M. C., & Barry, R. G. (2014). *The Arctic climate system*, (2nd ed.). Cambridge: Cambridge University Press.

Skogen, M. D., Budgell, W. P., & Rey, F. (2007). Interannual variability in Nordic seas primary production. *ICES Journal of Marine Science*, *64*(5), 889–898. https://doi.org/10.1093/icesjms/fsm063

Slagstad, D., Wassmann, P. F. J., & Ellingsen, I. (2015). Physical constrains and productivity in the future Arctic Ocean. *Frontiers in Marine Science*, *2*, 85. https://doi.org/10.3389/fmars.2015.00085

Smedsrud, L. H., Halvorsen, M. H., Stroeve, J. C., Zhang, R., & Kloster, K. (2017). Fram Strait sea ice export variability and September Arctic sea ice extent over the last 80 years. *The Cryosphere*, *11*(1), 65–79. https://doi.org/10.5194/tc-11-65-2017

Smedsrud, L. H., Sirevaag, A., Kloster, K., Sorteberg, A., & Sandven, S. (2011). Recent wind driven high sea ice area export in the Fram Strait contributes to Arctic sea ice decline. *The Cryosphere*, *5*(4), 821–829. https://doi.org/10.5194/tc-5-821-2011

Smith, S. L., Smith, W. O., Codispoti, L. A., & Wilson, D. L. (1985). Biological observations in the marginal ice zone of the East Greenland Sea. *Journal of Marine Research*, *43*(3), 693–717. https://doi.org/10.1357/002224085788440303

Somayajula, S. A., Devred, E., Bélanger, S., Antoine, D., Vellucci, V., & Babin, M. (2018). Evaluation of sea-surface photosynthetically available radiation algorithms under various sky conditions and solar elevations. *Applied Optics*, *57*(12), 3088. https://doi.org/10.1364/AO.57.003088

Søreide, J. E., Leu, E. V. A., Berge, J., Graeve, M., & Falk-Petersen, S. (2010). Timing of blooms, algal food quality and *Calanus glacialis* reproduction and growth in a changing Arctic. *Global Change Biology*, *16*(11), 3154–3163. https://doi.org/10.1111/j.1365-2486.2010.02175.x

Spreen, G., Kern, S., Stammer, D., & Hansen, E. (2009). Fram Strait sea ice volume export estimated between 2003 and 2008 from satellite data. *Geophysical Research Letters*, *36*, L19502. https://doi.org/10.1029/2009GL039591

Steele, M., & Ermold, W. (2015). Loitering of the retreating sea ice edge in the Arctic Seas. *Journal of Geophysical Research: Oceans*, *120*, 7699–7721. https://doi.org/10.1002/2015JC011182

Sverdrup, H. U. (1953). On conditions for the vernal blooming of phytoplankton. *Journal du Conseil*, *18*(3), 287–295.

Taylor, M. H., Losch, M., Wenzel, M., & Schröter, J. (2013). On the sensitivity of field reconstruction and prediction using empirical orthogonal functions derived from Gappy data. *Journal of Climate*, *26*(22), 9194–9205. https://doi.org/10.1175/JCLI-D-13-00089.1

Tremblay, J. É., Anderson, L. G., Matrai, P., Coupel, P., Bélanger, S., Michel, C., & Reigstad, M. (2015). Global and regional drivers of nutrient supply, primary production and CO_2 drawdown in the changing Arctic Ocean. *Progress in Oceanography*, *139*, 171–196. https://doi.org/10.1016/j.pocean.2015.08.009

Vavrus, S. J., Holland, M. M., Jahn, A., Bailey, D. A., & Blazey, B. A. (2012). Twenty-first-century arctic climate change in CCSM4. *Journal of Climate*, *25*(8), 2696–2710. https://doi.org/10.1175/JCLI-D-11-00220.1

Wassmann, P., Duarte, C. M., Agustí, S., & Sejr, M. K. (2011). Footprints of climate change in the Arctic marine ecosystem. *Global Change Biology*, *17*(2), 1235–1249. https://doi.org/10.1111/j.1365-2486.2010.02311.x

Wu, B., Wang, J., & Walsh, J. E. (2006). Dipole anomaly in the winter Arctic atmosphere and its association with sea ice motion. *Journal of Climate*, *19*(1), 210–225. https://doi.org/10.1175/JCLI3619.1